Static Green's functions for a bisected coaxial cavity

Stefan Rossegger
CERN, CH-1211 Geneva, Switzerland
Stefan.Rossegger@cern.ch

and

Institut für Theoretische Physik - Computational Physics
Technische Unisersität, A-8010 Graz, Austria

August 25, 2009

CERN-OPEN-2009-009
25/08/2009

Abstract

This paper deals with the three-dimensional potential equation in cylindrical coordinates and its Green's function for geometry close to a rather uncommon Time Projection Chamber field-cage, namely a bisected coaxial cavity. The methods used to derive the Green's function for a coaxial cavity (see [CERN-OPEN-2009-003]) were adapted to deduce novel representations for a bisected geometry, where the additional Dirichlet conditions in ϕ have to be fulfilled. The necessary modifications are described in detail. In combination, these three novel representations allow fast converging calculations of the electric field components and therefore for any desired space charge configuration within this cavity.

KEYWORDS: Panda TPC, Green's function, bisected coaxial cavity,

1 Introduction

In [1], three different representations of the Green's function for a geometry close to a typical Time Projection Chamber (TPC) field-cage, namely a coaxial cavity, were derived. In combination, these three representations allow fast converging calculations of the potential and the electric field for nearly any position of the point charge and therefore for any desired space charge configuration within such geometry (e.g. the ALICE TPC [2]).

In contrast to typical TPCs, which are basically radially symmetric, the PANDA experiment aims for a TPC geometry which is bisected into two semi-circles in azimuthal direction [3]. In order to derive the corresponding static Green's functions, which provide non-oscillating electrical field representations for such a bisected coaxial cavity, the periodic boundary conditions in the azimuthal (ϕ) direction have to be replaced by a Dirichlet boundary condition:

$$\bar{\Phi}(0) = \bar{\Phi}(\epsilon) = 0 \tag{1}$$

whereas ϵ represents the opening angle of one wedge-shaped half of the TPC in the (r, ϕ)-plane.

Following the naming convention as used in [1], the proposed dimensions of the PANDA TPC are, inner radius $a = 0.15\ m$, outer radius $b = 0.42\ m$, length $L = 1.5\ m$ and opening angle $\epsilon = 170^\circ = 17/18 \cdot \pi$ (see [3, p.115]).

In order to derive the corresponding Green's function we use the approach as described in [1]. In the following, equations from this reference are referred to by using the general notation (R.#).

2 Adapted Green's functions for a bisected coaxial cavity

In contrast to the periodic boundary conditions in ϕ, as used for a coaxial cavity, the Dirichlet conditions as shown in equ.(1) do not force the separation constant α to be an integer any more. For the representations as they follow from equation (R.4), the solution of the Helmholtz equation in ϕ can be fulfilled by

$$\bar{\Phi}(\phi) = A_m \sin(\alpha_m \phi) \tag{2}$$

with $\alpha_m = m\pi/\epsilon$ and $m \in \mathrm{Z}$. Following the formalism of equation (R.29), we get the Fourier representation of the delta distribution in ϕ, which is

$$\delta(\phi - \phi')) \;=\; \sum_{m=1}^{\infty} \frac{\sin(\alpha_m \phi)\sin(\alpha_m \phi')}{N_{mn}^2} \quad \text{with} \quad N_{nm}^2 \;=\; \int_0^{\epsilon} \sin^2(\alpha_m \phi) d\phi = \frac{\epsilon}{2}. \tag{3}$$

This implies two major changes in the Greens functions as presented in (R.23) and (R.36). Firstly, the order of the Bessel functions m has to be replaced by α_m and secondly, the former Fourier representations of the delta distribution in ϕ as given in (R.15) and (R.28) have to be replaced by (3). The resulting Greens functions are given in (4) and (6).

For the representation by ordinary Bessel functions, which provides a fast converging representation of the electrical field component in z direction, we get:

$$G(r,\phi,z;r',\phi',z') = \frac{2}{\epsilon}\sum_{m=1}^{\infty}\sum_{n=1}^{\infty}\sin(\alpha_m\phi)\sin(\alpha_m\phi')\frac{R_{mn}(r)R_{mn}(r')}{\bar{N}_{mn}^2}\frac{\sinh(\beta_{mn}z_<)\sinh(\beta_{mn}(L-z_>))}{\beta_{mn}\sinh(\beta_{mn}L)}. \quad (4)$$

The solution of the Bessel differential equation, which fulfills the boundaries on $r = a$ and $r = b$, is then:

$$R_{mn}(r) = Y_{\alpha_m}(\beta_{mn}a)J_{\alpha_m}(\beta_{mn}r) - J_{\alpha_m}(\beta_{mn}a)Y_{\alpha_m}(\beta_{mn}r) \quad (5)$$

This implies small changes in the normalization term $\bar{N}_{mn}^2$ as well as in the calculation of the corresponding zeros β_{mn}.

For the representation by modified Bessel functions, which allows a fast converging representation for the electrical field in r direction, we can write:

$$G(r,\phi,z;r',\phi',z') = \\ = \frac{4}{\epsilon L}\sum_{m=1}^{\infty}\sum_{n=1}^{\infty}\sin(\alpha_m\phi)\sin(\alpha_m\phi')\sin(\beta_n z)\sin(\beta_n z')\frac{R_{mn\,1}(r_<)R_{mn\,2}(r_>)}{I_{\alpha_m}(\beta_n a)K_{\alpha_m}(\beta_n b) - I_{\alpha_m}(\beta_n b)K_{\alpha_m}(\beta_n a)} \quad (6)$$

implying the corresponding changes of the order, now $\alpha_m = m\pi/\epsilon$, in $R_{mn\,1}(r_<)$ and $R_{mn\,2}(r_>)$, (R.22) and (R.33) respectively.

For the modification of the third representation (R.57), we follow the hint starting from equation (R.19), where we had to solve the one-dimensional time-independent diffusion equation. For the ϕ direction, we now find that

$$g_{mn} = \frac{\sinh(\mu_{nk}\phi_<)\sinh(\mu_{nk}(\epsilon-\phi_>))}{\mu_{nk}\sinh(\mu_{nk}\epsilon)}, \quad (7)$$

fulfills the Dirichlet boundary condition in ϕ with $\phi_<$ for $0 \le \phi' < \phi \le \epsilon$ and $\phi_>$ for $0 \le \phi < \phi' \le \epsilon$.

Therefore, the Greens functions represented by modified Bessel functions of imaginary order, which allows a fast converging expression for the electrical field in ϕ direction, is

$$G(r,\phi,z;r',\phi',z') = \frac{2}{L}\sum_{k=1}^{\infty}\sum_{n=1}^{\infty}\frac{\sinh(\mu_{nk}\phi_<)\sinh(\mu_{nk}(\epsilon-\phi_>))}{\mu_{nk}\sinh(\mu_{nk}\epsilon)}\sin(\beta_n z)\sin(\beta_n z')\frac{R_{nk}(r)R_{nk}(r')}{N_{nk}^2}. \quad (8)$$

3 Results and comparison

The consistency of the three novel Green's functions for a bisected coaxial cavity, which fulfill the additional Dirichlet boundary conditions in ϕ (see equ.(1)), is demonstrated in figure (1). Furthermore, figures (2) to (4) display the non-oscillating behavior of the specially designed

representations in their dependence of the different variables when crossing the source point. The salient feature is: As regards precision a non-oscillating behavior of the function is more favorable than an oscillating one. Figure 5 shows the potential in the (r,ϕ)-plane for different positions of the point charge.

In summary, the special convergence properties of the representations as derived for a coaxial cavity are carried forward to the adapted representations to fulfill the boundary conditions of a bisected coaxial cavity. Together, the three novel Green's functions (4), (6) and (8) permit one the treatment of any space charge distribution within a bisected coaxial cavity such as the Panda TPC field cage. For example, the electric field components due to a charge distribution constant within a volume of $(0.2 \leq r \leq 0.3, 0.5 \leq \phi \leq 1.0, 0.5 \leq z \leq 1.0)$ are plotted in figure 6.

References

[1] S. Rossegger, *Static Green's functions for a coaxial cavity including an innovative representation.*, CERN-OPEN-2009-003, (2009).

[2] ALICE TPC Collaboration, TPC Technical Design Report, CERN-LHCC-2000-001, (2000).

[3] The PANDA Collaboration, *Technical Progress Report for PANDA*, http://www-panda.gsi.de/, (2009).

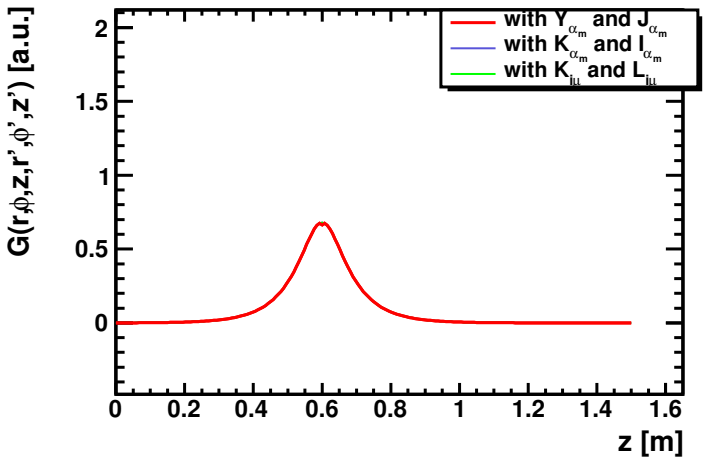

Figure 1: Representations (4), (6) and (8) as a function of z with $(r', \phi', z') = (0.3, 1.2, 0.6)$ and $(r, \phi) = (0.25, 1)$. The summation limits for m and n were set to 40. All three representations coincide since the domain of the plot is chosen outside the region of slow convergence.

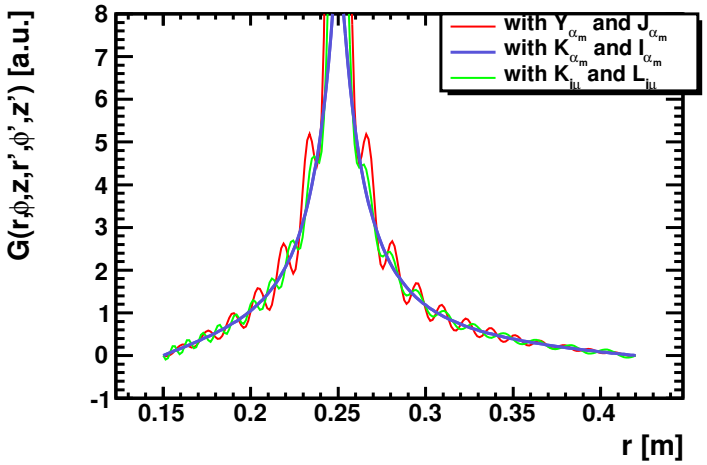

Figure 2: Representations (4), (6) and (8) as functions of the radius r with $r' = 0.25$ m ($z = z' = 0.5$ m, $\phi = \phi' = 1.0$ rad). The summation limits for m and n were set to 40. Solution (6) does not oscillate.

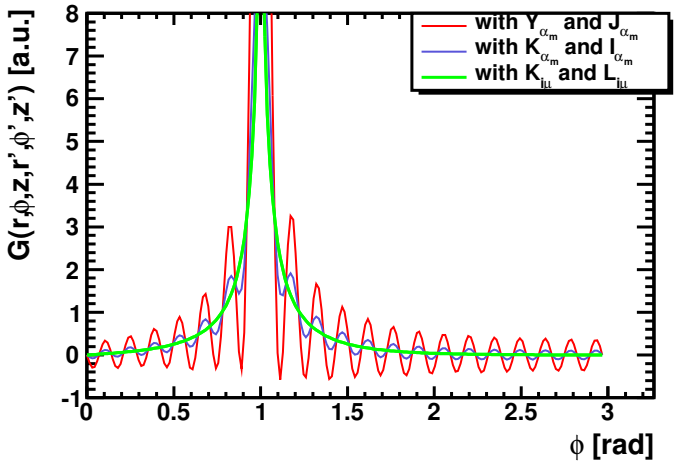

Figure 3: Solution (4), (6) and (8) as a function of ϕ with ϕ' at 1.0 rad ($r = r' = 0.25$ m, $z = z' = 0.5$ m). The summation limits for m and n were set to 40. Solution (8) does not oscillate.

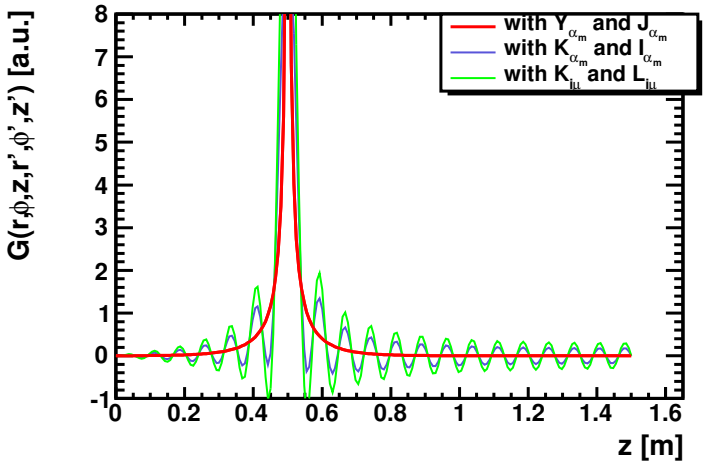

Figure 4: Solution (4), (6) and (8) as a function of the z axis with z' at 0.5 m ($r = r' = 0.25$ m, $\phi = \phi' = 1.0$ rad). The summation limits for k and n were set to 40. Solution (4) does not oscillate.

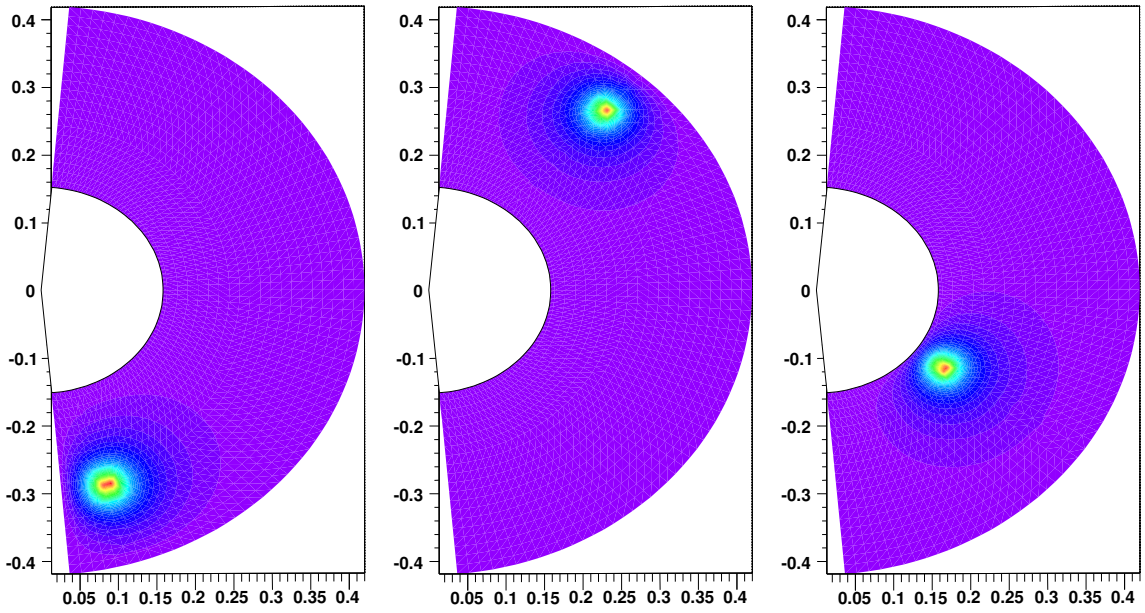

Figure 5: $(r, \phi)-$contour plots of the Green's function (8) at $z = z'$; Summation limits set to 40; $a = 0.15$ m, $b = 0.42$ m, $L = 1.5$ m

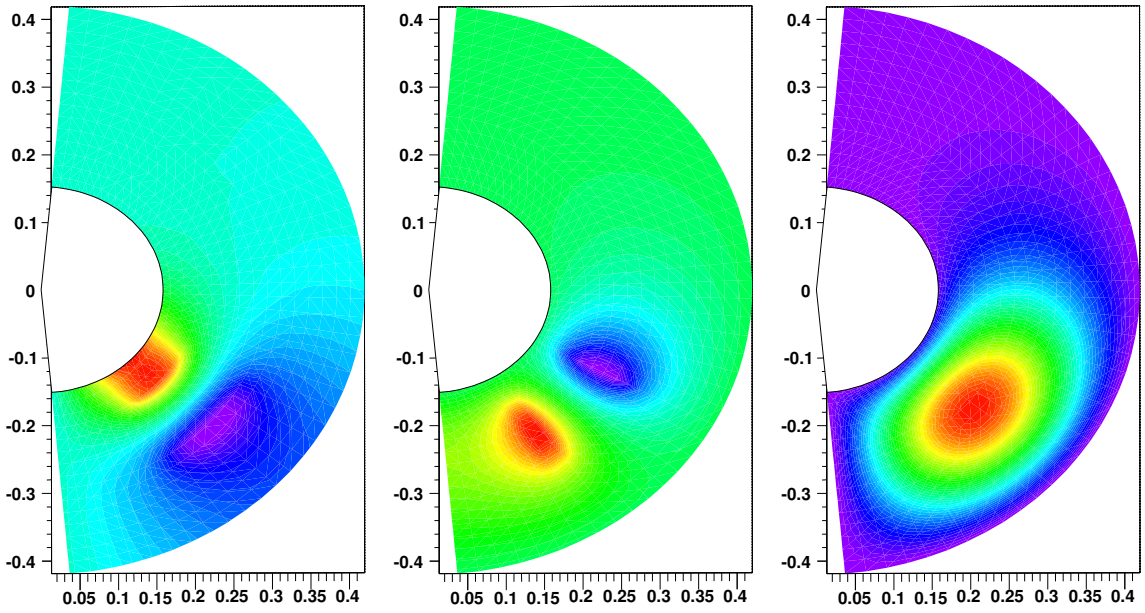

Figure 6: Electrical fields in (r, ϕ) plane at $z = 0.7$ m for a constant space charge distribution within the region $(0.2 \leq r \leq 0.3, 0.5 \leq \phi \leq 1.0, 0.5 \leq z \leq 1.0)$. *left:* E field in radial direction (E_r) *middle:* E field in azimuthal direction (E_ϕ) *right:* E field in longitudinal direction (E_z). Summation limits set to 40; $a = 0.15$ m, $b = 0.42$ m, $L = 1.5$ m